Available online at www.sciencedirect.com
SCIENCE DIRECT®
Acta Materialia 54 (2006) 3343–3349
Acta MATERIALIA
www.actamat-journals.com

Low-thermal-conductivity plasma-sprayed thermal barrier coatings with engineered microstructures

Amol D. Jadhav [a], Nitin P. Padture [a,*], Eric H. Jordan [b], Maurice Gell [b], Pilar Miranzo [c], Edwin R. Fuller Jr. [d]

[a] *Department of Materials Science and Engineering, The Ohio State University, Columbus, OH 43210, USA*
[b] *Institute of Materials Science, University of Connecticut, Storrs, CT 06269, USA*
[c] *Instituto de Cerámica y Vidrio, CSIC,Cantoblanco, 28049 Madrid, Spain*
[d] *Ceramics Division, Materials Science and Engineering Laboratory, National Institute of Standards and Technology, Gaithersburg, MD 20899, USA*

Received 23 January 2006; received in revised form 9 March 2006; accepted 13 March 2006
Available online 5 June 2006

Abstract

The solution precursor plasma spray (SPPS) process has been used to deposit ZrO_2–7 wt.% Y_2O_3 thermal barrier coatings (TBCs) that contain alternate layers of low and high porosities (layered-SPPS). The thermal conductivity of the layered-SPPS coating is found to be lower than those of both a SPPS coating with distributed porosity and an air-plasma-sprayed coating of the same composition, in the temperature range 100–1000 °C. Analytical and object-oriented finite element (OOF) models have been used to analyze the experimental thermal conductivity data. The OOF model is better at describing the experimentally measured thermal conductivities than the analytical model, and the OOF model captures accurately the effect of real microstructures on the thermal conductivities of these plasma-sprayed TBCs.

Keywords: Plasma spraying; Coatings; Ceramics; Thermal conductivity; Finite element analysis

1. Introduction

Air plasma spray (APS) is a low-cost method for depositing ceramic thermal barrier coatings (TBCs) used to protect and to insulate hot-section metallic components in gas turbine and diesel engines [1–3]. The ubiquitous "splat" boundaries and microcracks in APS TBCs that run parallel to the metal/ceramic interface are highly effective in reducing the thermal conductivity of APS TBCs. However, the "splat" boundaries and the microcracks are also the source of weakness in APS TBCs, limiting their in-service spallation life [4,5].

To that end, a new plasma-based coatings deposition method – solution precursor plasma spray (SPPS) – has been developed and used to deposit highly durable TBCs [6–8]. In the SPPS process, an aqueous chemical precursor feedstock that results in a ZrO_2–7 wt.% Y_2O_3 (7YSZ) ceramic solid solution is injected into the plasma jet. This is in contrast to the APS process, where ceramic powder is used as the feedstock [9,10]. By virtue of the deposition mechanisms that are fundamentally different from those in the APS process, the microstructures of SPPS TBCs are vastly different from those of APS TBCs. The key microstructural features of the SPPS TBCs are: (i) distributed porosity; (ii) through-thickness vertical cracks; and (iii) lack of large-scale "splat" boundaries/cracks. The porosity and the through-thickness vertical cracks impart strain-tolerance to the TBC, while the lack of large-scale splat boundaries effectively toughens the TBC [8].

Although SPPS TBCs have been found to be highly durable in cyclic heating/cooling laboratory tests where thermal gradients were not involved, SPPS TBCs have thermal conductivities higher than APS TBCs [6]. This

* Corresponding author. Tel.: +1 614 247 8114; fax: +1 614 292 1537.
E-mail address: padture.1@osu.edu (N.P. Padture).

1359-6454/$30.00
doi:10.1016/j.actamat.2006.03.024

provides the motivation for reducing the thermal conductivities of SPPS TBCs for use in engine environments where steep thermal gradients across TBCs are desired.

In this context, we exploit the versatility of the SPPS process in depositing layered TBCs with microstructures engineered for reducing the thermal conductivity. Here we use the SPPS method to deposit 7YSZ TBCs with alternating layers of low and high porosities. The layered-SPPS TBCs are found to have thermal conductivities lower than those of both SPPS TBCs and APS TBCs of the same chemical composition. Analytical modeling and the object-oriented finite element (OOF) method are used to analyze microstructural effects on the thermal conductivities of the TBCs studied here. This is in an effort to support and to guide microstructural design of low-thermal-conductivity TBCs.

2. Experimental

Both SPPS and APS coatings were deposited, using the same direct-current 9MB plasma torch (Sulzer Metco, Westbury, NY) attached to a six-axis robotic arm, on grit-blasted, plasma-preheated (preheating temperature ~200 °C) 304 stainless steel disk substrates (diameter 25.4 mm, thickness 4 mm). For SPPS coatings the feedstock used was an aqueous precursor solution of zirconium and yttrium salts (Inframat Corp., Farmington, CT), to result in a solid solution of 93 wt.% ZrO_2 and 7 wt.% Y_2O_3 (7YSZ) in the coating. Two different types of SPPS coatings were deposited under different processing conditions, one to result in a coating with distributed porosity and the other to result in alternate layers of low and high porosities. For APS coatings, ceramic powder feedstock (Metco 204NS, Sulzer Metco, Westbury, NY) of a similar composition was used. The final coating thickness for all three types of coatings (APS, SPPS, and layered-SPPS) deposited here was 1.3 mm.

Cross-sections of the three types of coatings were cut and polished to a 1 μm final finish using routine metallographic techniques. The cross-sectional coating microstructures were observed using optical microscopy and a scanning electron microscopy (SEM; Quanta, FEI, Hillsboro, OR). Quantitative image analysis was performed on the SEM images (at least 25 micrographs per coating) using a image-analysis software (Clemex Vision, Clemex Technologies Inc., Longueil, Canada) and stereological formulations [11].

Thermal conductivity measurements were performed using a method described in earlier studies [6,12,13]. Briefly, free-standing coatings of as-sprayed APS, SPPS, and layered-SPPS were obtained by dipping the specimens in a 40% HNO_3 solution for 2 h, where the acid attacked selectively the partially attached metal/ceramic interfaces. These were then cut and ground into plates ($8.8 \times 8.8 \times 1\ mm^3$). Thermal diffusivity ($\kappa$) of each plate specimen was measured at various temperatures in the range 100–1000 °C during heating using the laser-flash technique (Thermaflash 2200, Holometrix, Bedford, MA) in Ar atmosphere. Prior to thermal diffusivity measurements, the front and the back faces of each specimen were coated with two thin layers of gold and carbon, respectively, to prevent direct transmission of the laser beam through the translucent specimens. Appropriate corrections were made in the thermal diffusivity calculations to account for the presence of these layers. The precision of the thermal diffusivity measurements was ±5%. The specific heat capacities (c) as a function of temperature for 7YSZ was obtained from a previous study [6]. Densities (ρ) of the plate specimens were measured using the Archimedes principle, with deionized water as the immersion medium. The thermal conductivity (k) is given by $k = \kappa\rho c$.

3. Results and discussion

3.1. Microstructures

Figs. 1(a) and (b) show SEM micrographs of the APS coating at low and high magnification, respectively, showing splats, splat boundaries/cracks, vertical microcracks, and pores. These microstructures are similar to those documented in the APS coatings literature [9,10]. The density of the APS coating was found to be 5.16 g cm^{-3}, or 0.15 volume-fraction porosity (ϕ), assuming the density of fully dense 7YSZ to be 6.07 g cm^{-3}.

Figs. 2(a) and (b) show SEM microstructures of the SPPS coating at low and high magnification, respectively.

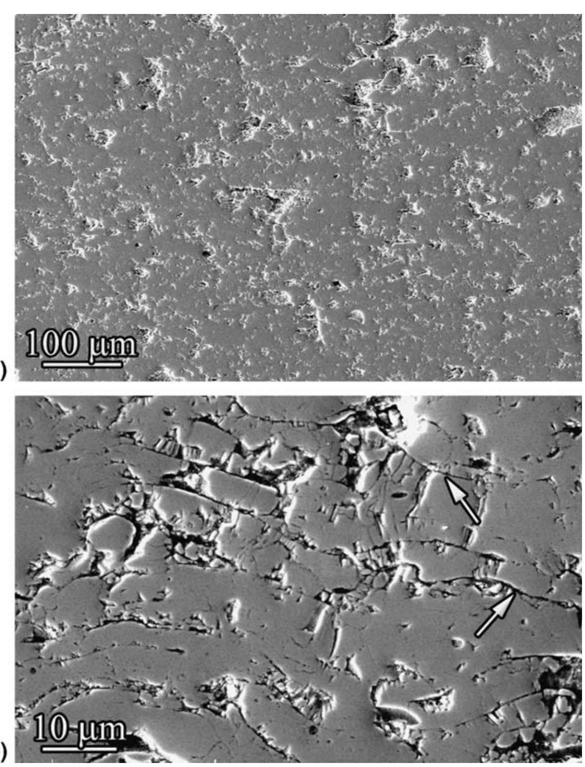

(a) (b)

Fig. 1. SEM micrographs of the APS coating at: (a) low magnification; and (b) high magnification. Arrows in (b) indicate splat boundaries.

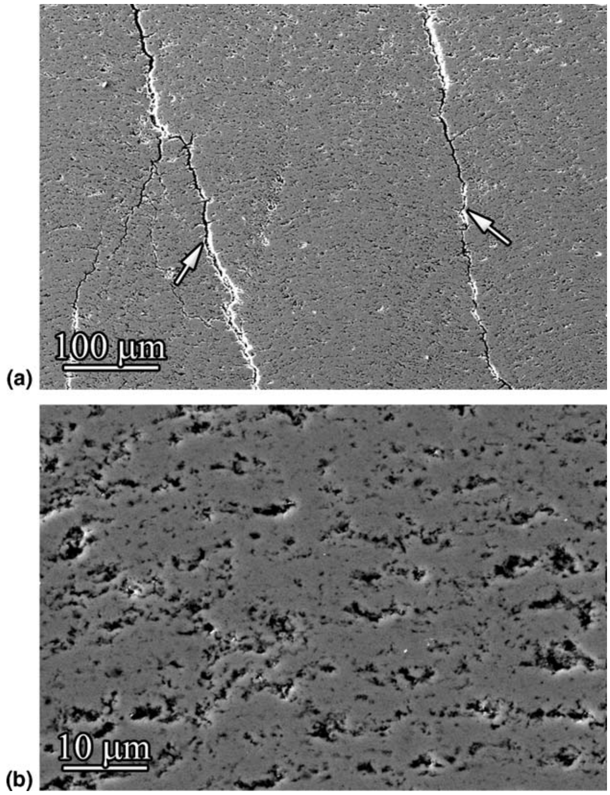

Fig. 2. SEM micrographs of the SPPS coating at: (a) low magnification; and (b) high magnification. Arrows in (a) indicate vertical cracks.

Note the absence of large splats and splat boundaries/cracks that are always present in the APS coatings. The porosity in the SPPS coating appears to be distributed, but with a somewhat horizontal texture. The SPPS coatings are also characterized by through-thickness vertical cracks (Fig. 2(a)).

Figs. 3(a)–(c) show microstructures of the layered-SPPS coating at low (optical), medium (SEM), and high (SEM) magnifications, respectively. The interleaved low- and high-porosity layers, and the through-thickness vertical cracks, are clearly visible in Fig. 3(a). Figs. 3(b) and (c) show that the pores within the high-porosity layers are not continuous. The dashed lines in Fig. 3(c) mark the approximate locations of the high- and low-porosity layers, where the high-porosity layers contain elongated pores primarily, while the low-porosity layers contain mainly round pores.

For analytical modeling of microstructural effects on thermal conductivity, detailed image analysis of the SPPS coatings was performed with the following assumptions: (i) elongated pores are approximated by disks, with diameter d and thickness t, and aspect ratio $d/t > 1.25$; and (ii) round pores of $d/t < 1.25$ are approximated by spheres. In the case of layered-SPPS coatings the following assumptions are made: (i) high-porosity layers of thickness L_{Disk} contain only disk-shaped pores; and (ii) low-porosity layers of thickness L_{Sphere} contain only spherical pores. All disk-shaped pores are assumed to be parallel to the substrate/coating interface and perpendicular to the heat flux. These assumptions, depicted schematically in Fig. 4, are essential for striking a balance between simplifying the representation of complex microstructures for analytical modeling and capturing the key microstructural characteristics.

Table 1 summarizes the data from the detailed image analyses of the SPPS and layered-SPPS coatings.

The densities of the SPPS and the layered-SPPS coatings were measured to be 4.73 and 4.13 g cm^{-3}, respectively. The corresponding porosity volume fractions (ϕ) of 0.22 and 0.32 for SPPS and layered-SPPS coatings, respectively, compare with those estimated from image analysis (Table 1).

3.2. Thermal conductivity: experimental data

Fig. 5 shows a plot of thermal conductivity as a function of temperature for APS, SPPS, and layered-SPPS coatings. Thermal conductivity data for fully dense, hot-pressed 7YSZ from a previous study [12] are included in Fig. 5 for comparison. Overall, although the thermal conductivities in Fig. 5 are seen to decrease with temperature, they are not a strong function of temperature, which has been attributed to strong phonon scattering in zirconia ceramics [14–16].

The thermal conductivity values for the APS coating (0.8–1.0 W m^{-1} K^{-1}) in Fig. 5 compare with the data obtained by others for 7YSZ APS coatings [17–19]. The thermal conductivities of the SPPS coating (1.0–1.2 W m^{-1} K^{-1}) are found to be higher than those of the APS coating. Note that the SPPS coating is thermally more resistive than TBCs fabricated using electron-beam physical vapor deposition (EB-PVD); thermal conductivities of 7YSZ EB-PVD coatings are in the range 1.5–2.0 W m^{-1} K^{-1} (not shown here) [18–20]. In Fig. 5 it can be seen clearly that the layered-SPPS coating is thermally more resistive (thermal conductivity 0.7–0.8 W m^{-1} K^{-1}) than both the APS and the SPPS coatings in the temperature range studied.

3.3. Thermal conductivity: analytical modeling

The reduced thermal conductivity of the porous coatings, relative to the dense 7YSZ, is considered to be solely due to the missing dielectric medium in the form of pores. This is described by the Maxwell equation for materials with spherical, non-interacting pores of volume-fraction porosity ϕ_{Sphere} [21]:

$$\frac{k_{\mathrm{Spherical\ pores}}}{k_{\mathrm{Dense}}} = 1 - \frac{3}{2}\phi_{\mathrm{Sphere}} \tag{1}$$

The pores are assumed to be non-conducting, and their sizes are too large to scatter phonons [16]. Scattering of radiation by pores is also neglected because the radiation penetration depth of plasma-sprayed coatings is negligible (~10 µm) [22]. However, the coatings studied here contain non-spherical pores, and therefore we consider a model

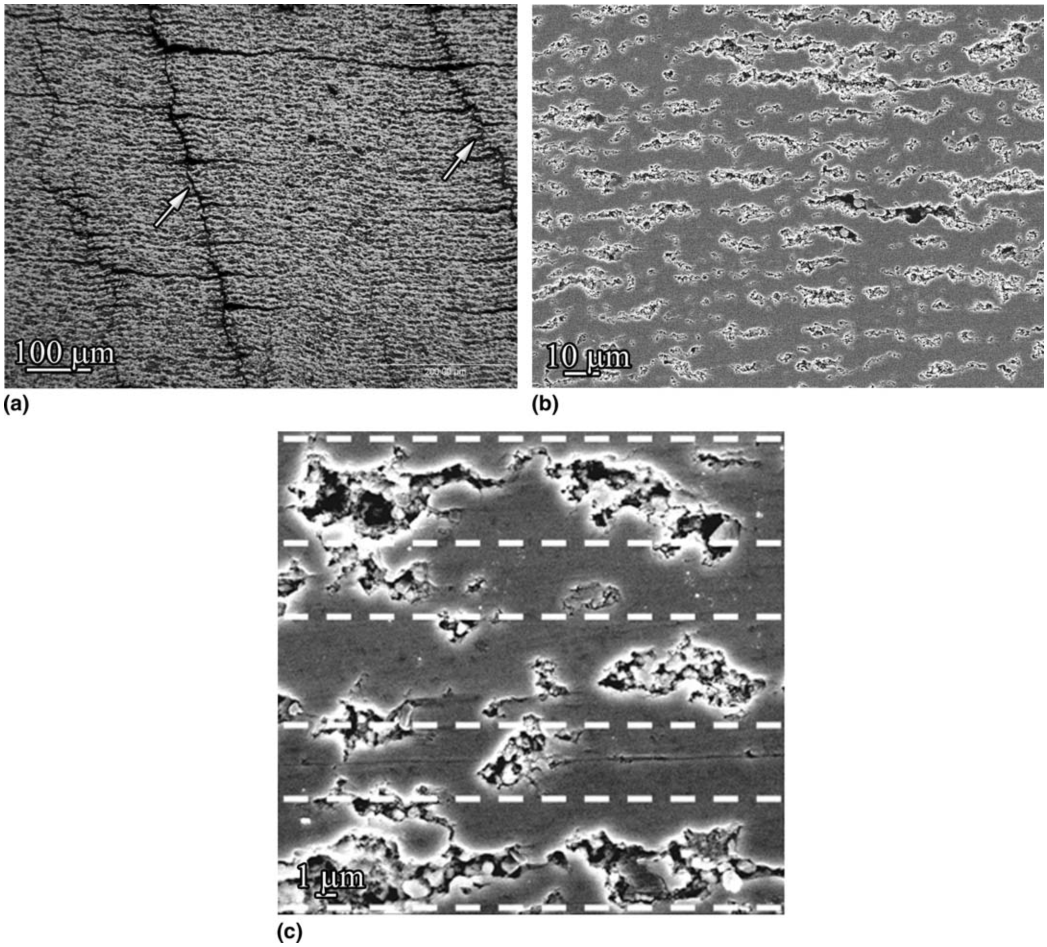

Fig. 3. (a) Low-magnification optical micrograph of the layered-SPPS coating showing alternate layers and vertical cracks (arrows). SEM micrographs at (b) low and (c) high magnification, showing the alternate layers of low and high porosities. Dashed lines in (c) demarcate approximate boundaries between low- and high-porosity layers.

proposed by Kachanov and co-workers [23,24] that takes into account non-spherical morphology of pores. For disk-shaped pores aligned normal to the heat flux (Fig. 4) the thermal conductivity reduction is given by [23–25]

$$\frac{k_{\text{Disk Pores}}}{k_{\text{Dense}}} = 1 - \left(\frac{2\phi_{\text{Disk}}}{\pi}\right)\left(\frac{d}{t}\right) \tag{2}$$

Consider the SPPS coating which contains both spherical and disk-shaped pores. The combined effect of the two different types of porosities on the thermal conductivity SPPS is given by [26]

$$k_{\text{SPPS}} = \frac{1}{2}\left\{f_4\left(\frac{\phi_{\text{Disk}}}{1-\phi_{\text{Sphere}}}\right)f_3(\phi_{\text{Sphere}}) + f_3\left(\frac{\phi_{\text{Sphere}}}{1-\phi_{\text{Disk}}}\right)f_4(\phi_{\text{Disk}})\right\}k_{\text{Dense}} \tag{3}$$

where f_3 and f_4 are functions representing Eqs. (1) and (2), respectively. Using Eqs. (1)–(3) and the microstructural data from Table 1, the calculated thermal conductivity of the SPPS coating is plotted in Fig. 5. The calculated thermal conductivities are within 12.7% of the experimental values, and they are consistently lower than the experimental values. This could be due to various reasons, including (i) overestimation of the porosities in the coatings and (ii) assumption of all disk-shaped pores being aligned normal to the heat flux, which may not be strictly valid.

Consider the layered-SPPS coating, which contains alternating layers of spherical pores (low porosity) and disk-shaped pores (high porosity) (Figs. 3 and 4). Thus, the conductivity of the layered-SPPS coating is given by

$$k_{\text{Layered-SPPS}} = \left(\frac{f_3(\phi_{\text{Sphere}})f_4(\phi_{\text{Disk}})(L_{\text{Sphere}} + L_{\text{Disk}})}{f_3(\phi_{\text{Sphere}})L_{\text{Disk}} + f_4(\phi_{\text{Disk}})L_{\text{Sphere}}}\right)k_{\text{Dense}} \tag{4}$$

Using Eqs. (1), (2) and (4), and the microstructural data from Table 1, the calculated thermal conductivities of the layered-SPPS coating are also plotted in Fig. 5. The agreement between the calculated and the experimental values is within 11.3%, which is better than that in the SPPS-coating case. Once again, the calculated values are consistently lower than the experimental values, which can also be attributed to the reasons mentioned above. Nevertheless, the agreement between the calculated and experimental thermal conductivities is noteworthy considering that there are no adjustable parameters in Eqs. (1), (2) and (4).

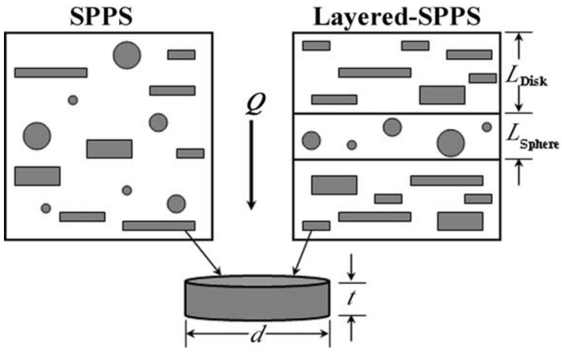

Fig. 4. Schematic showing the different types of porosities (spherical and disk-shaped) present in the SPPS and the layered-SPPS coatings. The direction of heat flow (Q), and the thicknesses of the low (L_{Sphere}) and high (L_{Disk}) porosities are indicated. The disk-shaped pores are assumed to have a diameter d and thickness t.

Table 1
Results of the microstructural characterization of the SPPS and layered-SPPS coatings

Microstructural parameter	Symbol	SPPS	Layered-SPPS
Porosity volume fraction from disk-shaped pores	ϕ_{Disk}	0.17	0.24
Porosity volume fraction from spherical pores	ϕ_{Sphere}	0.07	0.06
Total porosity volume fraction ($\phi_{Disk} + \phi_{Sphere}$)	ϕ	0.24	0.30
Average aspect ratio of disk-shaped pores	d/t	2.84	3.34
Average thickness of high-porosity layer (μm)	L_{Disk}	–	6
Average thickness of low-porosity layer (μm)	L_{Sphere}	–	4
Average vertical crack spacing (μm)	W	170	300
Average vertical crack gap thickness (μm)	u	0.11	0.13

Note that the vertical cracks in both SPPS and layered-SPPS coatings have a negligible effect on the thermal conductivity, as determined using the expression of Lu et al. (Eq. (18a) in Ref. [25]) and the data in Table 1.

The thermal conductivity of the APS coating was not analyzed using the models discussed above because the microstructural parameters for that coating could not be quantified satisfactorily. Instead, the newly developed OOF method [27] was used to analyze the thermal conductivity of the APS coating. For comparison, the thermal conductivities of the SPPS and layered-SPPS coatings were also analyzed using the OOF method.

3.4. Thermal conductivity: OOF

OOF is a relatively new finite element-based approach that combines data in the form of microstructures with fundamental material data (such as elastic modulus or thermal conductivity of the constitutive phases) as a basis for understanding the behavior of complex materials [27]. Although the current version of OOF (a public domain software [28]) is limited to two-dimensional microstructures, it has been used successfully in analyzing elastic modulus [29], thermal stresses [30,31], thermal expansion [29], and thermal conductivities [32] of complex materials, including APS TBCs.

In this study the inputs for two-dimensional OOF were digitized SEM images of the APS, SPPS, and layered-SPPS coatings. The microstructures were converted into binary images consisting of only two distinct phases: 7YSZ and pores (Ar gas). The 7YSZ phase was assigned dense-7YSZ thermal conductivity from Fig. 5 for a given temperature. Thermal conductivity of Ar was calculated using the dilute gas approximation [33] for the entire temperature range. The thermal conductivity of gas phase confined to pores has been found to be different from its conductivity in open space. The following analytical expression can be used to estimate thermal conductivity (k_{Gas}) of a gas phase in pores [22]:

$$k_{Gas} = \frac{k^0_{Gas}}{1 + \frac{BT}{d_t P}} \tag{5}$$

where k_{Gas} is the conductivity of Ar gas in open space, T is the absolute temperature, P is the pressure, B is a constant (2.5×10^{-5} Pa m K^{-1}), and d_t is the pore thickness. Average values of d_t for the APS, the SPPS, and the layered-SPPS coatings were measured to be 0.3, 0.6 and 1.9 μm, respectively.

The binary images were then meshed using an adaptive meshing procedure, which allowed the subdivision of the elements and movement of nodes to conform to the

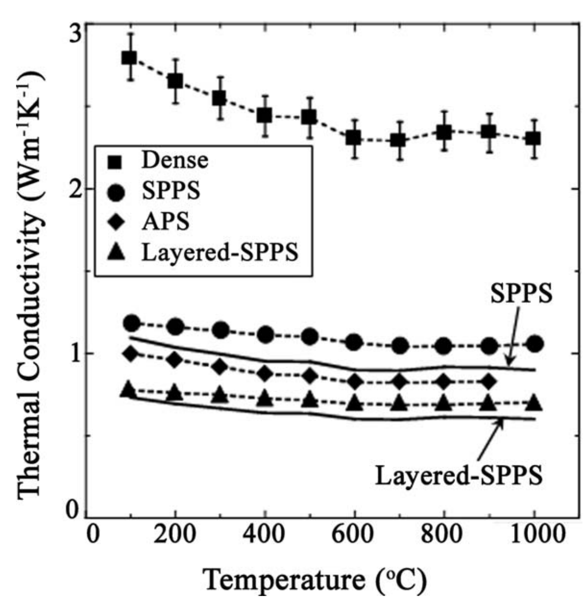

Fig. 5. Thermal conductivity as a function of temperature. The symbols represent experimentally measured data, and they are connected with dashed lines. Error bars represent ±5%, which are about the size of the symbols for SPPS, layered-SPPS, and APS coatings. The solid lines represent results from the analytical modeling for SPPS and layered-SPPS coatings. Experimental data for the dense 7YSZ is from Ref. [12].

microstructure. This helps in minimizing the energy functional parameter of the mesh, which can be further reduced by an "annealing" procedure at the conclusion of the meshing operation. A finer mesh is created at the 7YSZ/pore interfaces where higher temperature gradients are expected, as shown in Fig. 6 for a small portion of the layered-SPPS coating microstructure. A typical OOF mesh for the layered-SPPS coatings consisted of up to 220,000 triangular elements for the 7YSZ phase, and up to 75,000 elements for pores, depending on the complexity of a specific microstructure. The top and the bottom of the meshed micrographs were assigned constant temperatures of T_1 and T_2, such that a thermal gradient of 10 °C ($T_1 - T_2$) is set up across the meshed micrographs, in the direction of the expected heat flow in an actual TBC. The two vertical sides of the micrographs were kept adiabatic. The resultant heat flux was used to obtain the average thermal conductivity of the microstructure. Fig. 7 shows an example of a microstructure (layered-SPPS) with superimposed thermal gradient.

The thermal conductivity results from the OOF analysis for the APS, SPPS, and layered-SPPS coatings are plotted in Fig. 8. In the cases of the APS, SPPS, and layered-SPPS coatings the agreements between the experimental data and the OOF results are within 8.5%, 2.1%, and 6.0%, respectively. These agreements are better than those obtained using analytical modeling, despite that fact that OOF is a two-dimensional model. This can be attributed to fact that "real" microstructures are used as input in OOF, instead of the approximated, ideal microstructures used in the analytical modeling. This demonstrates the utility of OOF in capturing accurately the effect of real microstructures on the thermal conductivities of plasma-sprayed TBCs.

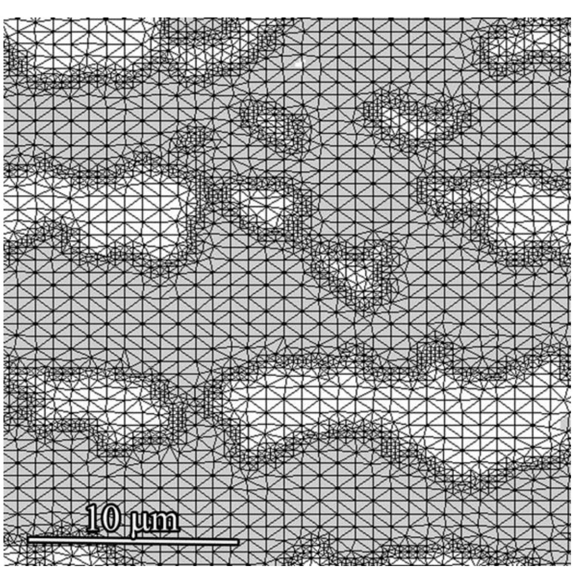

Fig. 6. OOF mesh of a small region of the layered-SPPS microstructure. The dark and the light regions are 7YSZ and pores, respectively. Note the finer mesh near the 7YSZ/pore boundaries.

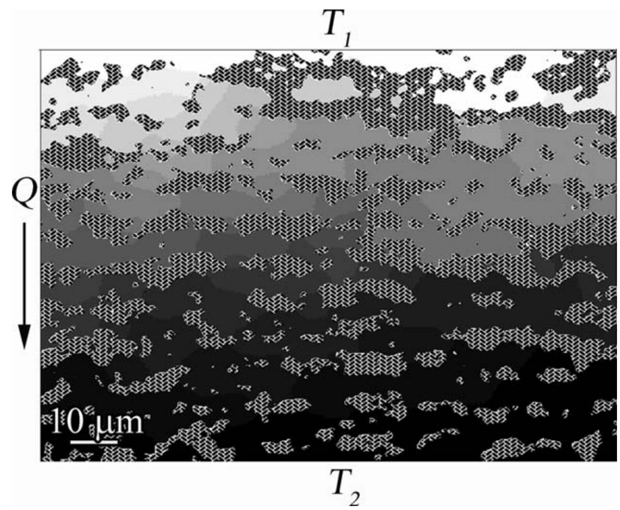

Fig. 7. OOF microstructure of the layered-SPPS coating with a superimposed thermal gradient of ($T_1 - T_2$). The cross-hatched region represents porosity.

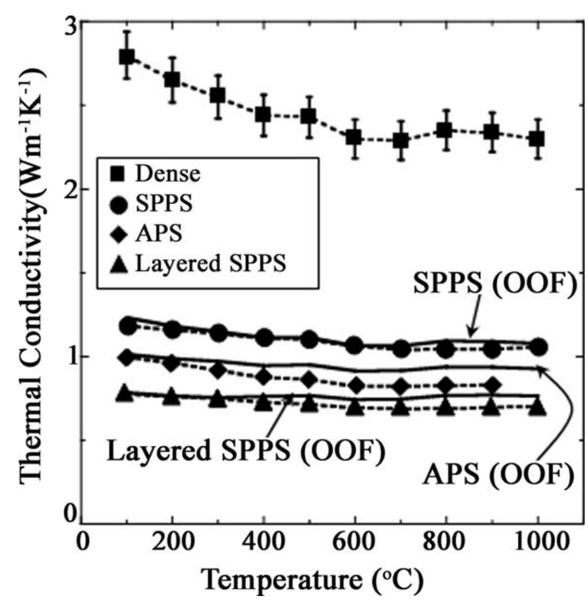

Fig. 8. Thermal conductivity as a function of temperature. The symbols represent experimentally measured data, and they are connected with dashed lines. Error bars represent ±5%, which are about the size of the symbols for SPPS, layered-SPPS, and APS coatings. The solid lines represent results from OOF modeling for APS, SPPS, and layered-SPPS coatings. Experimental data for the dense 7YSZ is from Ref. [12].

4. Summary

The microstructures of SPPS TBCs have been tailored to contain alternate layers of high and low porosities (layered-SPPS), in an effort to reduce the thermal conductivity of SPPS TBCs. The thermal conductivities of the 7YSZ layered-SPPS coating are found to be lower than those of both the SPPS coating and the APS coating of the same composition, in the temperature range 100–1000 °C. Analytical modeling and OOF have been used to analyze the experimental thermal conductivity data. The OOF model is better at describing the experimentally measured thermal conductivities than the analytical model, and the OOF model captures accurately the effect of real microstructures on the thermal conductivities of these plasma-sprayed TBCs.

Acknowledgements

The authors thank Dr. X. Ma and Mr. J. Roth for providing the precursors and depositing the coatings; Drs. M. Osendi, J. Shyue, A. Vasiliev, F. Wu, and L. Xie for experimental assistance; Prof. P. Klemens for fruitful discussions; and Dr. E. Lemmon for helpful discussions regarding thermal conductivity of Ar gas and for providing a beta version of the NIST Reference Fluid Thermodynamic and Transport Properties database. This publication was prepared with the support of the US Department of Energy (DoE), Office of Fossil Energy, National Energy Technology Laboratory (Grant No. 03-01-SR107). Any opinions, findings, conclusions, or recommendations expressed herein are those of the authors and do not necessarily reflect the views of the DoE.

References

[1] Jones RL. In: Stern KH, editor. Metallurgical and ceramic coatings. London: Chapman & Hall; 1996. p. 194.
[2] Evans AG, Mumm DR, Hutchinson JW, Meier GH, Pettit FS. Prog Mater Sci 2001;46:505.
[3] Padture NP, Gell M, Jordan EH. Science 2002;296:280.
[4] Rabiei A, Evans AG. Acta Mater 2000;48:3963.
[5] Schlichting KW, Padture NP, Jordan EH, Gell M. Mater Sci Eng 2003;A342:120.
[6] Padture NP, Schlichting KW, Bhatia T, Ozturk A, Cetegen B, Jordan EH, et al. Acta Mater 2001;49:2251.
[7] Gell M, Xie L, Ma X, Jordan EH, Padture NP. Surf Coat Technol 2004;177–178:97.
[8] Jadhav A, Padture NP, Wu F, Jordan EH, Gell M. Mater Sci Eng A 2005;405:313.
[9] Powlowski L. The science and engineering of thermal spray coatings. New York (NY): Wiley; 1995.
[10] Herman H, Sampath S, McCune R. MRS Bull 2000;25:17.
[11] Russ JC. Practical stereology. New York (NY): Plenum Press; 1986.
[12] Wu J, Wei X, Padture NP, Klemens PG, Gell M, Garcia E, et al. J Am Ceram Soc 2002;85:3031.
[13] Wu J, Padture NP, Klemens PG, Gell M, Garcia E, Miranzo P, et al. J Mater Res 2002;17:3193.
[14] Hasselman DPH, Johnson LF, Bentsen LD, Syed R, Lee HL, Swain MV. Am Ceram Soc Bull 1987;66:799.
[15] Klemens PG. In: Wilkes KE, Dinwiddie RB, Graves RS, editors. Thermal conductivity, vol. 23. Lancaster (PA): Technomic; 1996. p. 209.
[16] Schlichting KW, Padture NP, Klemens PG. J Mater Sci 2001; 36:3003.
[17] Eaton HE, Linsey JR, Dinwiddie RB. In: Tong TW, editor. Thermal conductivity, vol. 22. Lancaster (PA): Technomic; 1994. p. 289.
[18] Zhu D, Miller RA. Ceram Eng Sci Proc 2002;23:457.
[19] Clarke DR, Phillpot SR. Mater Today 2005;8:22.
[20] Levi CG. Curr Opin Solid State Mater Sci 2002;8:77.
[21] Maxwell JC. A treatise on electricity and magnetism. Oxford: Clarendon Press; 1904.
[22] Golosnoy IO, Tsipas SA, Clyne TW. J Therm Spray Technol 2005;14:205.
[23] Shafiro B, Kachanov M. J Appl Phys 2000;87:8561.
[24] Sevostianov I, Kachanov M. Mater Sci Eng A 2001;297:235.
[25] Lu TJ, Levi CG, Wadley HNG, Evans AG. J Am Ceram Soc 2001;84:2937.
[26] Cernuschi F, Ahmaniemi S, Vuoristo P, Mantyla T. J Eur Ceram Soc 2004;24:2657.
[27] Langer SA, Fuller Jr ER, Carter WC. Comput Sci Eng 2001;3:15.
[28] http://www.ctcms.nist.gov/oof/.
[29] Chawla N, Patel BV, Koopman M, Chawla KK, Saha R, Patterson BR, et al. Mater Charact 2003;49:395.
[30] Hsueh CH, Haynes JA, Lance MJ, Becher PF, Ferber MK, Fuller Jr ER, et al. J Am Ceram Soc 1999;82:1073.
[31] Saigal A, Fuller Jr ER. Comput Mater Sci 2001;21:149.
[32] Wang Z, Kulkarni A, Deshpande SA, Nakamura T, Herman H. Acta Mater 2003;51:5319.
[33] Lemmon EW, Jacobsen RT. Int J Thermophys 2004;25:21.